Low and medium energy deuteron-induced reactions on ^{27}Al

P. Bém,* E. Šimečková, and M. Honusek
Euratom/IPP.CR Fusion Association, Nuclear Physics Institute, 25068 Řež, Czech Republic

U. Fischer and S. P. Simakov
Euratom/FZK Fusion Association, Forschungszentrum Karlsruhe, Hermann-von-Helmholtz-Platz, 1, 76344 Eggenstein-Leopoldshafen, Germany

R. A. Forrest
Euratom/UKAEA Fusion Association, Culham Science Centre, Abingdon OX14 3DB, United Kingdom

M. Avrigeanu,† A. C. Obreja, F. L. Roman, and V. Avrigeanu
'Horia Hulubei' National Institute for Physics and Nuclear Engineering, P. O. Box MG-6, Bucharest-Magurele, Romania
(Received 30 January 2009; published 30 April 2009)

The activation cross sections of (d,p), $(d,2p)$, and $(d,p\alpha)$ reactions on ^{27}Al were measured in the energy range from 4 to 20 MeV using the stacked-foils technique. Following a previous extended analysis of elastic scattering, breakup, and direct reaction of deuterons on ^{27}Al, for energies from 3 to 60 MeV, the preequilibrium and statistical emissions are considered in the same energy range. Finally, all deuteron-induced reactions on ^{27}Al including the present data measured up to 20 MeV deuteron energy are properly described due to a simultaneous analysis of the elastic scattering and reaction data.

DOI: 10.1103/PhysRevC.79.044610 PACS number(s): 24.10.Ht, 24.60.Dr, 25.45.−z, 27.30.+t

I. INTRODUCTION

The complexity of deuteron-induced reactions from the lowest energies and the variety of reactions that occur at incident energies below the nucleon-binding energy due to the very small (2.2 MeV) deuteron binding energy, compared to the nucleon-induced reactions, has recently been well described [1]. The role of proton- and deuteron-induced reactions in the assessment of induced radioactivity of accelerator components (elements such as Al, Cu, Fe, Cr, Nb, etc.) is of great interest. The IFMIF (International Fusion Material Irradiation Facility) accelerator needs cross section data in the energy range from the threshold (2–10 MeV) up to 40 MeV, for both deuterons and protons. To investigate the first important nuclides relevant to the IFMIF, irradiation experiments were carried out [2,3] using the variable-energy cyclotron U-120M of the Nuclear Physics Institute Řež. The experimental section of the present work deals with the cross sections of reaction products, investigated by irradiation of aluminium foils with a deuteron beam of 20 MeV.

In the energy range up to 20 MeV there is no optical model potential (OMP) global parameter set [4] that describes reasonably the scattering data as well as the total reaction cross sections over a wide range of nuclei [5]. Because the OMP is a basic ingredient of almost all nuclear model studies, there is thus an increased uncertainty in the calculated deuteron-induced reaction cross sections. However, the weak binding of the deuteron leads to significant contributions of the breakup reaction channel. Thus, a detailed analysis of the deuteron elastic scattering and induced activation cross sections appeared essential for their consistent understanding [5,6]. Investigation of the OMP has also proven useful for providing a suitable input into actual engineering design activities in the energy range up to 50 MeV [7]. We consider in this work, along with a former related optical and direct reaction (DR) assessment [8], the statistical processes induced by deuterons on the ^{27}Al nucleus.

II. MEASUREMENTS

A. Samples and irradiations

The NPI variable energy cyclotron U-120M provides protons and deuterons at energies of 11–37 MeV and 11–20 MeV, respectively, in the negative-ion mode of acceleration. The energy is varied by relocating the position of an extracting foil. In every run, the energy was determined by a calculation procedure, comparing the results from activation- and Si-detector technique measurements with a resulting accuracy of 1%. The same relative uncertainty is used for the energy spread (FWHM) of the collimated beam at each reaction chamber position. In the present work, the energy of deuterons was 20.4 ± 0.2 MeV.

The cross section of deuteron-induced activation was measured by the stacked-foil technique. Stacks of high purity foils of natural Al and Cu (purity of 99.99%, Goodfellow product) were placed in a Faraday-cup type of reaction chamber and cooled during the irradiation. The cooling avoided the possible destruction of the thin foils by the beam current below 500 nA due to heating. The thickness of Al and Cu foils was 50 and 25 μm, respectively, determined by weighting with an

*bem@ujf.cas.cz
†mavrig@ifin.nipne.ro

accuracy of 2%. To check the consistency of measured data, two stacks of foils were utilized and irradiated in two different runs, A and B.

The current of the collimated incident beam in the reaction chamber was measured with a 5% accuracy. The history of the irradiation was determined by recording the current every 2 s. During the irradiation for the A and B runs, the current was kept constant at 90 and 330 nA for exposure times of 900 and 300 s, respectively.

Following a 10 min delay from the end of irradiations the γ rays from activated foils were measured by two calibrated HPGe detectors of 23 and 50% efficiency and of FWHM 1.8 keV at 1.3 MeV. Measured spectra were analyzed using the γ-spectroscopy method. To provide reliable corrections for the decay, the beam-current recorder and γ-ray spectrometer were synchronized in time. Activated isotopes were identified using nuclear decay data from Ref. [9]. By analyzing the spectra, the resulting specific activities at the end of irradiation were obtained. The uncertainty of 3% includes statistical errors and the uncertainty of the detector-efficiency calibration.

B. Calculation of cross sections and their errors

To enlarge the number of energy bins in the measured excitation functions and to check the internal consistency of the measured data, the foils were stacked with different Al vs Cu sequences in A and B runs. The mean deuteron energy, energy thickness, and straggling for each foil were determined using the SRIM 2003 code [10]. The overall thickness of the available 22 foil stacks covers the excitation-curve range from 20 to 6 MeV. The cross-section value for each foil was calculated in the standard way [11] using the number of incident deuterons, target atoms, and measured reaction products (corrected for the decay during the irradiation) (Table I).

Errors of experimental cross section data are composed of the foil-thickness uncertainty (2%) and a mean statistical error in the determination of specific activities (3%). The scale of excitation functions is known within an error of 5% (due to the uncertainty of beam-current integration). In Fig. 1, the excitation functions of cross sections determined in the runs A and B for reactions ^{27}Al$(d,2p)^{27}$Mg and ^{63}Cu$(d,2n)^{63}$Zn are shown. The overestimation of the data from run A over run B is clearly indicated within a factor of about 10% for both reactions. The scale factor of 0.95 was therefore applied to all data from run A which was carried out at a lower beam current (leading to larger relative uncertainty of current integration). Except for this small effect, the consistency of data measured at different runs is evident.

TABLE I. Measured reaction cross sections (mb) for deuterons incident on the ^{27}Al nucleus. The mean deuteron energy and resolution due to the thickness and straggling of each foil are shown. Statistical uncertainties are given in parentheses for the cross sections in units of the last digit.

Energy (MeV)	Reaction		
	^{27}Al$(d,p)^{28}$Al	^{27}Al$(d,2p)^{27}$Mg	^{27}Al$(d,p\alpha)^{24}$Na
3.38 (93)	210(9)	0.15(2)[a]	0.096(6)[a]
5.14 (73)	486(35)	0.17(1)[a]	0.100(12)[a]
6.28 (63)		0.17(1)[a]	0.095(5)[a]
7.55 (58)	419(33)	0.19(2)[a]	0.101(12)[a]
8.44 (53)	361(14)	0.29(2)	0.097(5)[a]
9.53 (50)	327(24)	0.59(4)	0.109(9)[a]
10.30 (47)	239(26)	1.36(4)	0.122(5)
11.26 (90)	207(14)	2.14(14)	0.283(21)
11.93 (43)		3.95(9)	0.916(43)
12.81 (42)	186(22)	5.84(37)	2.26(15)
13.41 (40)	159(6)	6.48(18)	4.61(36)
14.23 (39)	162(12)	8.74(57)	7.94(53)
14.79 (37)	146(25)	10.41(21)	12.02(38)
15.55 (37)	135(10)	12.29(80)	16.4(11)
16.08 (75)	132(10)	14.61(34)	21.0(11)
16.79 (36)		17.3(11)	26.4(16)
17.31 (36)		17.13(46)	30.2(21)
17.97 (35)		19.1(12)	34.6(23)
18.47 (35)		18.84(45)	43.0(14)
19.09 (34)		21.1(13)	42.1(28)
19.57 (34)	89.6(37)	21.76(48)	48.3(14)
20.18 (33)		21.7(14)	51.8(35)

[a]Cross-section values that are likely to be affected by neutrons generated into a foil behind the original one.

^{27}Al$(d,p)^{28}$Al ($T_{1/2} = 2.2414$ min). An attempt to determine cross sections for the ^{27}Al$(d,p)^{28}$Al reaction for the short-living nuclide ^{28}Al was also carried out. In Fig. 2(b), the overestimation of the previous data of Wilson *et al.* [13] over the present experiment (up to a factor of 2) is evident.

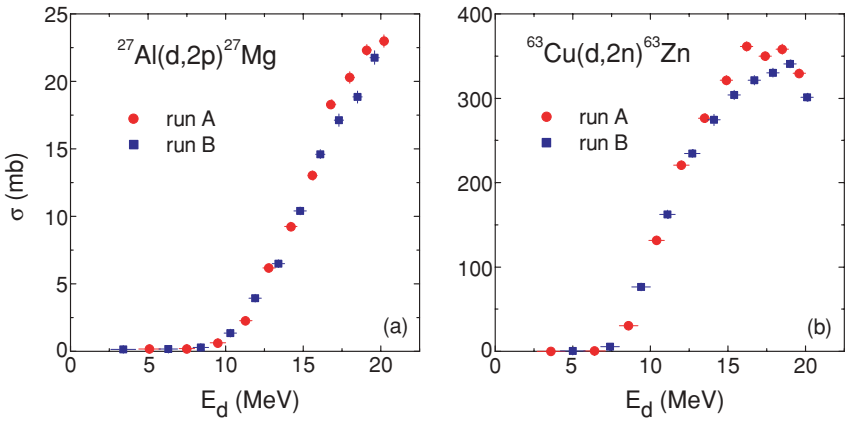

FIG. 1. (Color online) The excitation functions of cross sections determined in different runs A and B for the reactions ^{27}Al$(d,2p)^{27}$Mg and ^{63}Cu$(d,2n)^{63}$Zn. The overestimation of data from run A over run B is clearly indicated within a scale factor of about 10% for both reactions.

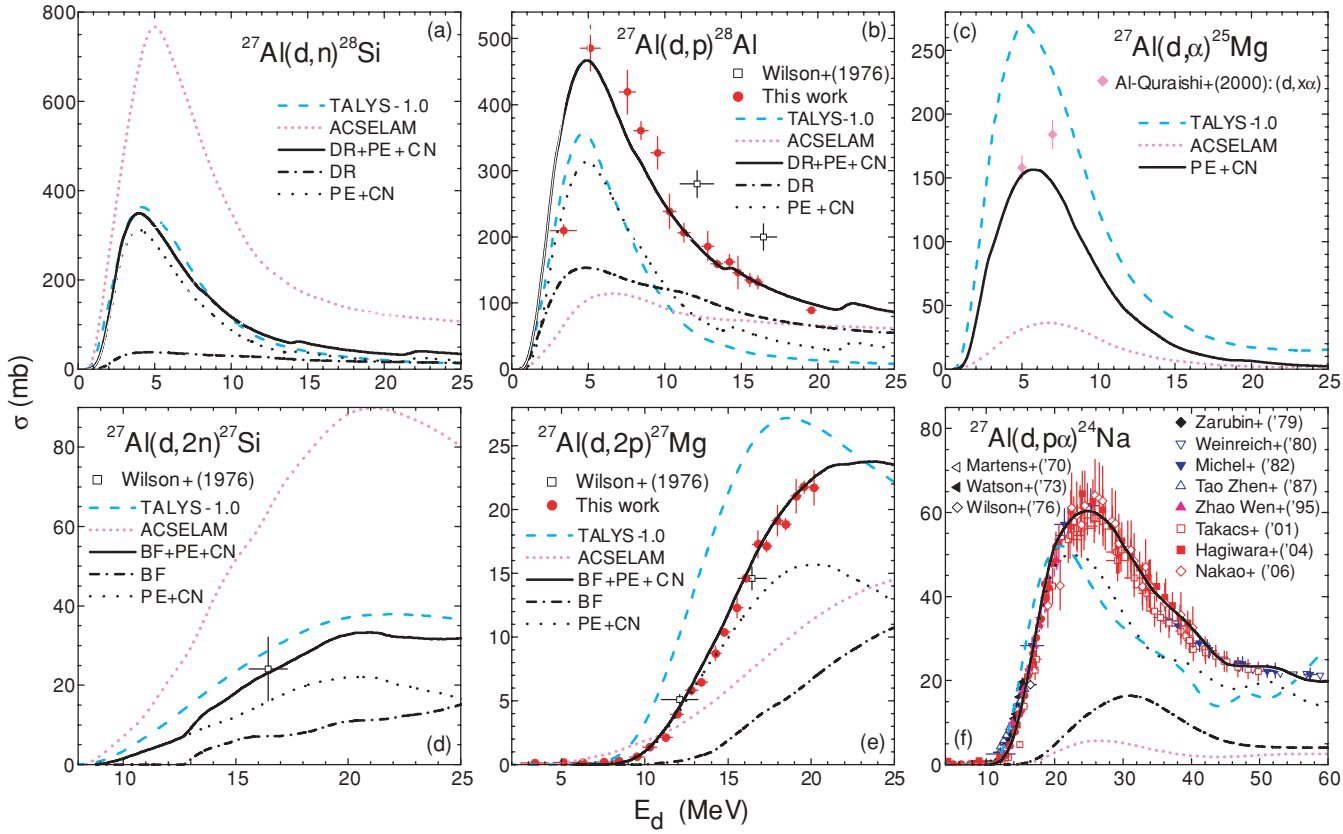

FIG. 2. (Color online) Comparison of measured (this work, solid circles, and Ref. [12]) and calculated reaction cross sections provided by the code TALYS (dashed curves); the library ACSELAM (short-dotted); and local analysis (solid) using the DR results (dash-dotted) for the (d,p) and (d,n) reactions and deuteron breakup for the $(d,2p)$, $(d,2n)$, and $(d,p\alpha)$ reactions and the PE + CN components (dotted).

No simple explanation could be found for this discrepancy taking into account the fairly good agreement of data for one other short-living nuclide, ^{27}Mg, measured with the thin-target technique [11] and the present stacked-foil technique.

^{27}Al$(d,2p)^{27}$Mg ($T_{1/2} = 9.458$ min). The cross section data for the formation of ^{27}Mg measured in the present experiment are shown in Fig. 2(e). The present cross section data for the ^{27}Al$(d,2p)^{27}$Mg reaction are seen to be in good agreement with the data from the only experiment carried out by Wilson *et al.* [13] at other energies by the thin-target technique.

^{27}Al$(d,p\alpha)^{24}$Na ($T_{1/2} = 14.959$ h). In Fig. 2(f), the present data are compared with a large set of data [12]. Detailed investigation of this uncertainty agreement has confirmed that the determination of the energy in present experiments is about 0.2 MeV, evaluated for the incident deuteron beam.

III. NUCLEAR MODEL ANALYSIS

A. Deuteron optical potential and breakup systematics

A previous extended analysis of elastic scattering and DR cross sections of deuterons on ^{27}Al nuclei, for deuteron energies from 3 to 60 MeV [8], was based on a semimicroscopic optical potential with a double-folding real part and phenomenological imaginary as well as spin-orbit terms. In a second step of that analysis, the imaginary and spin-orbit potential parameters were kept fixed while a full phenomenological OMP was obtained as needed for the usual model calculations. The advantage of having already determined at least half of the usual OMP parameters obviously increases the effectiveness of fitting the data. Based on the corresponding local OMP parameters at various incident energies, the average energy-dependent OMP parameters (Table II) have been obtained and applied successfully for a description of the experimental elastic scattering angular distributions and total reaction cross sections especially at deuteron energies from 5 to 20 MeV [8].

Further study has been concerned with the breakup processes, namely, the elastic breakup (EB) [14–16], in which the target nucleus remains in its ground state and none of the deuteron constituents interacts with it, and the inelastic breakup [14,15] or breakup fusion (BF) [16] where one of these deuteron constituents interacts with the target nucleus while the remaining one is emitted and eventually detected. The deuteron breakup peak energies of the emitted constituents are assumed to be described by Gaussian line shapes [17] with centroids as shown in Fig. 3(a). The analyses of proton-emission spectra and angular distributions from deuteron-induced reactions on nuclei from Al to Pb, at incident energies from 15 to 80 MeV [8], provided the energy- and mass-dependence of the total proton-emission breakup $\sigma_{\rm EB} + \sigma_{\rm BF}^{(p)}$

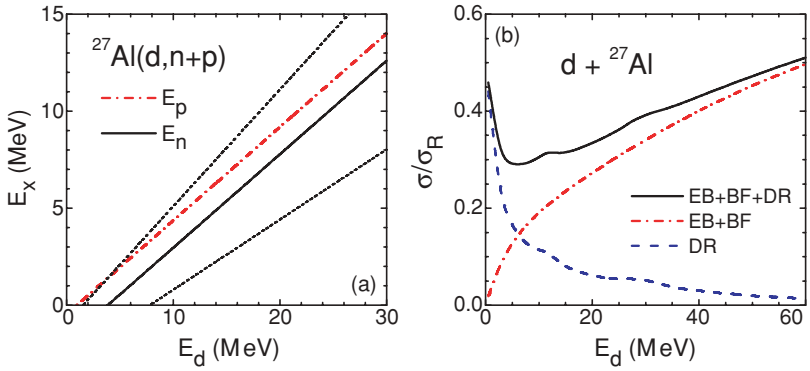

FIG. 3. (Color online) (a) The centroid E_x of assumed Gaussian line shape [17] for deuteron breakup peak energies of emitted neutrons (solid) and protons (dash-dotted) and the corresponding $E_n \pm \Delta$ values (dashed). (b) The sum (solid curve) of the ratios of deuteron breakup (dash-dotted) and stripping DR [8] (dashed) to the total reaction cross sections.

and the elastic breakup $\sigma_{\rm EB}$ cross sections (Eqs. (1) and (2), respectively, of Ref. [8]) versus the total reaction cross section σ_R. Assuming that the BF cross section for the proton emission is the same as that for the neutron emission $\sigma_{\rm BF}^{(n)}$, the total breakup reaction cross section, given by the sum $\sigma_{\rm EB} + 2\sigma_{\rm BF}^{(n)}$, is shown in Fig. 3(b) for the target nucleus ^{27}Al and the energy range of present interest. At the same time it is compared with the corresponding DR contributions to the (d,p) and (d,n) reaction cross sections [8], which have a similar total weight around 5 MeV.

B. Statistical particle emission

While the interaction of deuterons with the target nuclei proceeds largely by DR processes below and around the Coulomb barrier, other reaction mechanisms like preequilibrium emission (PE) or evaporation from the fully equilibrated compound nucleus (CN) become important when the incident energy is increased. The related cross sections have been analyzed in this work by using the default model parameters (except for the deuteron OMP in Table II) of the widely used computer code TALYS [18] as well as a local consistent parameter set developed in calculations with the PE + CN code STAPRE-H [19] taking into account also the breakup and DR results discussed above. The local analysis results obviously have a higher accuracy while the global predictions may be useful for an understanding of unexpected differences between measured and calculated cross sections. The main assumptions and parameters involved in this work for the sets of global and local calculations have recently been described elsewhere [20], only some points specific to the mass range $A < 30$ are given here.

The deuteron phenomenological optical model parameter set given in Table II has been used for the incident channel. The neutron optical potential of Koning and Delaroche [21] for ^{28}Si, used by default in TALYS, has been checked for a description of the total neutron cross section on ^{28}Si at the low energies involved within evaporation from the CN. It was found necessary to replace the constant real potential diffusivity $a_V = 0.668$ fm by the energy-dependent form $0.518 + 0.015E$ up to 10 MeV, leading to a decrease of $\sim$11% of the total neutron cross section in agreement with the most recent data [12] and evaluation [22]. The proton optical potential [21] for ^{27}Al has, however, been found to describe well the measured ^{27}Al$(p,n)^{27}$Si reaction cross sections available for incident energies up to $\sim$15 MeV. Finally, the optical potential of McFadden and Satchler [23] was used for calculation of the α-particle transmission coefficients. The same OMP parameter sets were employed within both the PE generalized [19] Geometry-Dependent Hybrid (GDH) model [24] and the CN statistical model.

The nuclear level densities were derived on the basis of the back-shifted Fermi gas (BSFG) formula [25], for the

TABLE II. The parameters of the deuteron optical potential.

Potential depths (MeV)		Geometry parameters (fm)	
$V_R = 84.4 - 0.27E$		$r_R = 1.30$	
		$a_R = 0.871 - 0.0083E$,	$E < 11$
		$= 0.78$,	$E > 11$
$W_V = -12.7 + 0.455E$		$r_V = 1.30$	
		$a_V = 0.88$	
$W_D = 14.4 + 0.57E$,	$E < 15$	$r_D = 1.61$,	$E < 9.4$
$= 28.2 - 0.348E$,	$E > 15$	$= 1.695 - 0.009E$,	$9.4 < E < 27.2$
		$= 1.45$,	$E > 27.2$
		$a_D = 0.772 - 0.026E$,	$E < 11.8$
		$= 0.465$,	$E > 11.8$
$V_{\rm SO} = 7.33 - 0.029E$		$r_{\rm SO} = 1.07$	
		$a_{\rm SO} = 0.66$	

excitation energies below the neutron binding energy, with small adjustments of the parameters a and Δ [26] obtained by a fit of more recent experimental low-lying discrete levels [27] and s-wave nucleon resonance spacings D_0 [28]. Above the neutron binding we took into account the washing out of shell effects within the approach of Ignatyuk *et al.* [29] and Junghans *et al.* [30] and using the method of Koning and Chadwick [31] for fixing the appropriate shell correction energy. A transition range from the BSFG formula description to the higher energy approach has been chosen between the neutron binding energy and the excitation energy of 15 MeV, mainly to have a smooth connection. However, the spin distribution has been determined by a variable ratio I/I_r of the nuclear moment of inertia to its rigid-body value : between 0.5 for ground states, 0.75 at the neutron binding energy, and 1 around the excitation energy of 15 MeV. Concerning the particle-hole state density, which for the PE description plays the same role as the nuclear level density for statistical model calculations, a composite formula [32] was used within the GDH model with no free parameter except for the α-particle state density $g_\alpha = A/10.36\ \mathrm{MeV}^{-1}$ [33].

Formally, no free parameter is involved for the PE description within the corresponding generalized GDH model except for α-particle emission, the above-mentioned s.p.l. density, and the preformation probability φ [33] with the value of 0.2 used in the present work. However, a particular comment concerns the initial configuration of excited particles (p) and holes (h) for deuteron-induced reactions in the present case. Similar careful studies [14,16,34,35] pointed out that 3p-1h or 2p-1h may be a suitable choice for this configuration. Our calculations show that the latter one gives the best agreement between the measured and calculated reaction cross sections.

IV. RESULTS AND DISCUSSION

In the present work, the activation cross sections of deuteron-induced reactions on ^{27}Al were measured in small energy bins in the energy range from 4 to 20 MeV using the stacked-foils technique. Excellent agreement between the present data and the recommended values from the EXFOR database was found for reaction $^{27}\mathrm{Al}\,(d,p\alpha)^{24}\mathrm{Na}$. New internally consistent data for excitation functions in this energy range were obtained for reactions $^{27}\mathrm{Al}\,(d,2p)^{27}\mathrm{Mg}$ and $^{27}\mathrm{Al}\,(d,p)^{28}\mathrm{Al}$ but there was found to be only in partial agreement with previous data [13] measured at other energies by the thin-target technique.

The comparison of the measured and calculated (d,n) and (d,p) reaction cross sections of ^{27}Al are shown in Figs. 2(a) and 2(b), including the present global and local analysis results as well as the ACSELAM library [36] results. For the local analysis both components of the final activation are shown, i.e., the DR cross sections provided by the code FRESCO and the PE + CN contributions supplied by STAPRE-H. The latter alone is rather close to the TALYS predictions while the ACSELAM data are about a factor >4 lower than the measured (d,p) reaction cross sections at the maximum of the excitation function, becoming lower than a factor of 2 at incident energies $\gtrsim$14 MeV, but they are about twice as high with respect to the other calculated results for the (d,n) reaction at lower energies. The local approach has led to much better agreement with the present (d,p) reaction data [2] especially due to the stripping DR contribution.

To obtain a complete description of the $(d,2p)$ and $(d,p\alpha)$ reaction cross sections, we have started by taking into account also the neutrons that, following the breakup proton emission, are absorbed in further interactions with the target nucleus. The cross section $\sigma_{\mathrm{BF}}^{(p)}$ [8] has been considered in this respect as shown in Figs. 4(a) and 4(b). It has been multiplied by the corresponding fraction leading to the above-mentioned reactions, which have been obtained by using the ratios of the most recently evaluated [22] (n,p) and (n,α) reaction cross sections, respectively, to the neutron total cross sections provided by the neutron global OMP [21]. These ratios have been expressed as a function of the deuteron incident energy while the Kalbach Walker [17] formula has been used

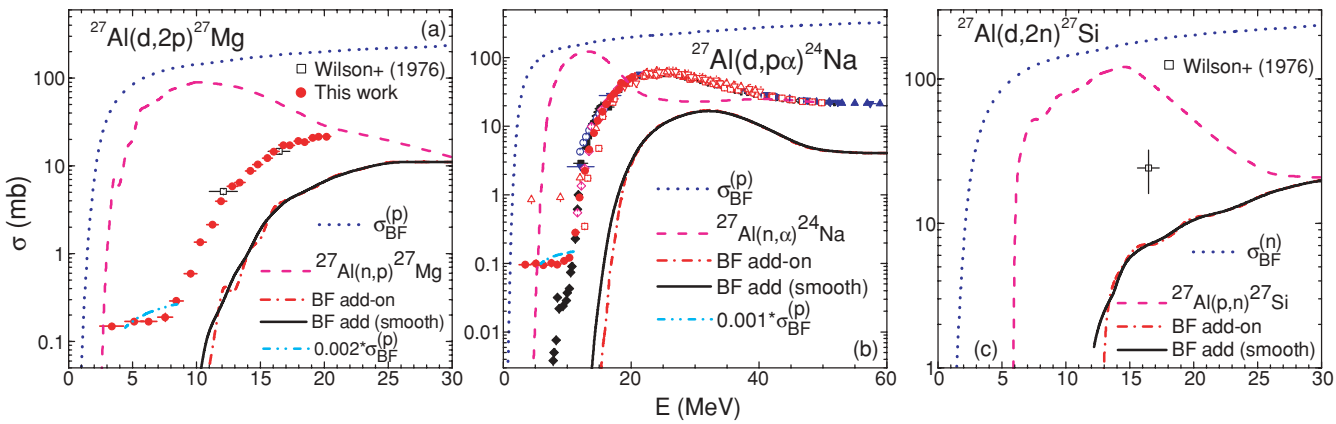

FIG. 4. (Color online) Comparison of measured data as in Fig. 2 and (a,b) the deuteron breakup neutron-emission cross section and (c) proton-emission cross section [8] (dotted curves), multiplied by the factors (a) 0.002 and (b) 0.001 (dash-dot-dotted); evaluated [22] cross sections of (a,b) the (n,p) and (n,α) reactions on ^{27}Al, respectively, as a function of neutron energy (dashed); and (c) calculated $^{27}\mathrm{Al}\,(p,n)^{27}\mathrm{Si}$ reaction cross sections as a function of proton energy; and the corresponding deuteron breakup corrections (dash-dotted) for (a,b,c), the $(d,2p)$, $(d,p\alpha)$, and $(d,2n)$ reactions on ^{27}Al, respectively, smoothed over 3 MeV (solid) as well.

for the centroid energy of the related breakup peaks. The quite large widths of the assumed Gaussian line shape of these peaks as showed in Fig. 3(a) emphasize, however, the broad approximation of this method. Therefore, the related contributions to the $(d,2p)$ and $(d,p\alpha)$ reaction cross sections provided by the above-mentioned multiplication have been additionally smoothed by using an average energy width of 3 MeV, with the results shown in Figs. 4(a) and 4(b). A similar procedure has been followed to obtain the contribution to the $(d,2n)$ reaction cross section due to the protons that, following the breakup neutron emission, are absorbed in further interactions with the target nucleus and described by the cross section $\sigma_{\mathrm{BF}}^{(n)}$ [Fig. 4(c)]. The only difference in this case concerns the $^{27}\mathrm{Al}\,(p,n)^{27}\mathrm{Si}$ reaction cross sections in the incident energy range up to 30 MeV, which has been obtained by the PE + CN calculation using the computer code STAPRE-H and the consistent local parameter set described above. All intermediary and ultimate reaction cross sections shown in Fig. 4 indicate that they may contribute up to 50% of the activation cross sections for deuteron incident energies of ~25 MeV.

The contribution due to the breakup proton, added to the PE + CN components provided by STAPRE-H, describe rather well the measured cross sections of the $(d,2p)$ and $(d,p\alpha)$ reactions as shown in Figs. 2(e) and 2(f). Similarly, the breakup neutron emission plays the same role for the $(d,2n)$ reaction as shown in Fig. 2(d). Their weight is obviously increasing with the incident energy because all reactions involved, following the deuteron breakup, within the second step of these processes have negative Q values. As a matter of fact, the exponential increase of these reaction cross sections just above the threshold energies is well described by the PE + CN components alone, but not the rather constant plateau around 0.1 and 0.2 mb over 4–5 MeV before the effective thresholds of the $(d,2p)$ and $(d,p\alpha)$ reactions, respectively. The same behavior, with shifts below 1 MeV, is common also to the TALYS and ACSELAM excitation functions. However, these yields below the effective reaction thresholds could be affected by neutrons generated into a foil behind the original one. Alternatively, the observed cross-section values below threshold may be due to the deuteron breakup, which has been taken into account only by means of the average energies of the related breakup energies shown in Fig. 3(a). Thus, for a given deuteron incident energy E_d, the energy of each breakup nucleon ranges from 0 to a maximum energy E_d-B_d, where B_d is the deuteron binding energy. Taking into account also the large widths of the assumed Gaussian line shapes of the deuteron breakup peak energies shown in Fig. 3(a), it follows that the lowest-energy plateau of the $(d,2p)$ and $(d,p\alpha)$ reactions may be related to similar breakup corrections as calculated and shown in Figs. 4(a) and 4(b) but corresponding to the largest energies of the breakup nucleon interacting with the target nucleus just above the breakup threshold. Consequently, in Figs. 4(a) and 4(b) are shown also the results obtained by using the cross section $\sigma_{\mathrm{BF}}^{(p)}$ multiplied by the average factors 0.002 and 0.001, respectively, in the energy ranges where this assumption could be meaningful. These factors stand for the ratios of the most recently [22] evaluated (n,p) and (n,α) reaction cross sections, respectively, to the neutron total cross sections, at the largest neutron energies available above the deuteron breakup threshold as well as the corresponding (n,p) and (n,α) reaction thresholds. Obviously, this is only a qualitative account of the $(d,2p)$ and $(d,p\alpha)$ reaction cross sections below the effective reaction thresholds, which is eventually able to describe them in addition to a possible effect of neutrons generated into a foil behind the original one.

A simpler analysis concerns the (d,α) reaction, which has no other breakup corrections except the corresponding decrease of the total reaction cross section. The DR effects have also been overlooked, due to the symmetrical experimental (d,α) reaction angular distributions [37] that are already reproduced by the PE + CN contributions. Thus the PE + CN components provide alone the corresponding activation excitation function, for which there is unfortunately no measured data. A check of the calculation accuracy has made use, however, in the frame of the local approach, of the $(d,x\alpha)$ spectra measured by Al-Quraishi *et al.* at 5 and 7 MeV [1]. We found that they correspond to α-particle production cross sections of 158 and 184 mb, respectively, shown in Fig. 2(c) with error bars not given in the original reference but coming out as typical of it. Within this error bar the local calculation is validated at lower energies, including additional contributions from the $(d,\alpha n + n\alpha)$ reactions of 7 and 2 mb, respectively. It follows that, around the maximum of this excitation function, the TALYS results are higher by ~70% than the measured data while the ACSELAM ones are lower by a factor of ~5. Additionally one should note the opposite case of TALYS for the $(d,p\alpha)$ reaction in Fig. 2(f) while the ACSELAM data are even lower. Finally, all activation data of deuteron-induced reactions on $^{27}\mathrm{Al}$ have been properly described, making obvious the usefulness of the concurrent description of all reaction channels as well as the simultaneous analysis of the deuteron elastic scattering and induced activation.

V. SUMMARY

The production cross sections of the nuclides $^{24}\mathrm{Na}$, $^{27}\mathrm{Mg}$, and $^{28}\mathrm{Al}$ were measured in the energy range from 4 to 20 MeV by irradiation of aluminium foils by a deuteron beam with an energy of 20 MeV. Excellent agreement between present data and the recommended values from the EXFOR database was found for the reaction $^{27}\mathrm{Al}\,(d,p\alpha)^{24}\mathrm{Na}$. New internally consistent data for excitation functions in this energy range were obtained for reactions $^{27}\mathrm{Al}\,(d,2p)^{27}\mathrm{Mg}$ and $^{27}\mathrm{Al}\,(d,p)^{28}\mathrm{Al}$ but there was found to be only partial agreement with previous data [13] measured at other energies by the thin-target technique.

Following a previous extended analysis of elastic scattering, breakup, and direct reaction of deuterons on $^{27}\mathrm{Al}$, for energies from 3 to 60 MeV [8], the preequilibrium and statistical emissions have been considered in the same energy range. The related cross sections have been analyzed by using the default model parameters (except for the deuteron OMP in Table II) of the widely used computer code TALYS as well as a local consistent parameter set developed in calculations with the PE + CN code STAPRE-H taking into account also the breakup and

DR results formerly discussed. The local approach has led to much better agreement with the present (d,p) reaction data especially due to the model calculation of the stripping DR contribution.

Consideration of the deuteron breakup plays a key role for the reaction channels adding a second emitted particle to a first one. Thus, to obtain a complete description of the $(d,2p)$ and $(d,p\alpha)$ reaction cross sections, we have taken into account also the neutrons which, following the breakup proton emission, are absorbed in further interactions with the target nucleus. The rather constant plateau around 0.1 and 0.2 mb over 4–5 MeV before the effective thresholds of the $(d,2p)$ and $(d,p\alpha)$ reactions, respectively, may well correspond to the lowest energies of the breakup neutron interacting with the target nucleus. Finally, all deuteron-induced reactions on ^{27}Al, including the present data measured at 20 MeV deuteron energy, have been properly described due to a simultaneous analysis of the elastic scattering and reaction data. A similar analysis will be further considered for evaluation of the deuteron activation of the copper isotopes [2] and other medium-mass nuclei.

ACKNOWLEDGMENTS

The authors are indebted to the operating crew of the U-120M Cyclotron for their ready assistance. This work was partly supported by the MTI CR under Contract 2A-1TP1/101; by the European Communities within the framework of the European Fusion Development Agreement under Contracts of Association between EURATOM and Forschungszentrum Karlsruhe, IPP.CR, and UKAEA; and by the CNCSIS-Bucharest under Contract PN-II No. 149/2007.

[1] S. I. Al-Quraishi, C. E. Brient, S. M. Grimes, T. N. Massey, J. Oldendick, and R. Wheeler, Phys. Rev. C **62**, 044616 (2000); EXFOR-C115 data file entry, dated 2005-01-24.

[2] P. Bém, L. Bittmann, V. Burjan, U. Fischer, M. Götz, M. Honusek, V. Kroha, J. Novák, S. Simakov, and E. Šimečková, in *Proceedings of the International Conference on Nuclear Data for Science and Technology, Nice, 2007*, edited by O. Bersillon *et al.* (EDP Sciences, Paris, 2008), p. 1003.

[3] S. P. Simakov, P. Bém, V. Burjan, U. Fischer, R. A. Forrest, M. Götz, M. Honusek, H. Klein, V. Kroha, J. Novák, A. Sauer, E. Šimečková, and R. Tiede, Fusion Eng. Des. **83**, 1543 (2008).

[4] J. M. Lohr and W. Haeberli, Nucl. Phys. **A232**, 381 (1974); W. W. Daehnick, J. D. Childs, and Z. Vrcelj, Phys. Rev. C **21**, 2253 (1980); H. An and C. Cai, Phys. Rev. C **73**, 054605 (2006).

[5] M. Avrigeanu, H. Leeb, W. von Oertzen, F. L. Roman, and V. Avrigeanu, in *Proceedings of the International Conference on Nuclear Data for Science and Technology, Nice, 2007*, edited by O. Bersillon *et al.* (EDP Sciences, Paris, 2008), p. 219.

[6] M. Avrigeanu, W. von Oertzen, U. Fischer, and V. Avrigeanu, Nucl. Phys. **A759**, 327 (2005).

[7] A. Ibarra, A. Möslang, R. Lässer, R. Ferdinand, R. Andreani, E. Surrey, B. Riccardi, V. Heinzel, H. Klein, U. Fischer, R. Forrest, and M. Gasparotto, Fusion Eng. Des. **82**, 2422 (2007); R. A. Forrest and I. Cook, Fusion Eng. Des. **82**, 2478 (2007).

[8] M. Avrigeanu, W. von Oertzen, R. A. Forrest, A. C. Obreja, F. L. Roman, and V. Avrigeanu, Fusion Eng. Des. (2009).

[9] S. Y. F. Chu, L. P. Ekström, and R. B. Firestone, The Lund/LBNL Nuclear Data, Search Version 2.0, February 1999, http://nucleardata.nuclear.lu.se/nucleardata/toi/.

[10] J. F. Ziegler, J. P. Biersack, and M. D. Ziegler, SRIM-The Stopping and Range of Ions in Matter, SRIM code, http://www.srim.org.

[11] K. Ochiai, M. Nakao, J. Hori, S. Sato, M. Yamauchi, N. S. Ishioka, and T. Nishitani, Fusion Eng. Des. **81**, 1459 (2006).

[12] Experimental Nuclear Reaction Data (EXFOR), www-nds.iaea.or.at/exfor.

[13] R. L. Wilson, D. J. Frantsvog, A. R. Kunselman, C. Détraz, and C. S. Zaidins, Phys. Rev. C **13**, 976 (1976).

[14] J. Kleinfeller, J. Bisplinghoff, J. Ernst, T. Mayer-Kuckuk, G. Baur, B. Hoffmann, R. Shyam, F. Rosel, and D. Trautmann, Nucl. Phys. **A370**, 205 (1981).

[15] G. Baur, F. Rosel, D. Trautmann, and R. Shyam, Phys. Rep. **111**, 333 (1984).

[16] M. G. Mustafa, T. Tamura, and T. Udagawa, Phys. Rev. C **35**, 2077 (1987).

[17] C. Kalbach Walker, TUNL Prog. Rep. XLII, 2002–2003, pp. 80–83, www.tunl.duke.edu/publications/tunlprogress/2003/.

[18] A. J. Koning, S. Hilaire, and M. C. Duijvestijn, in *Proceedings of the International Conference on Nuclear Data for Science and Technology, Nice, 2007*, edited by O. Bersillon *et al.* (EDP Sciences, Paris, 2008), p. 211.

[19] M. Avrigeanu and V. Avrigeanu, IPNE Report NP-86-1995, Bucharest, 1995, and references therein; Newslett. NEA Data Bank **17**, 22 (1995).

[20] M. Avrigeanu, S. Chuvaev, A. A. Filatenkov, R. A. Forrest, M. Herman, A. J. Koning, A. J. M. Plompen, F. L. Roman, and V. Avrigeanu, Nucl. Phys. **A806**, 15 (2008).

[21] A. J. Koning and J. P. Delaroche, Nucl. Phys. **A713**, 231 (2003).

[22] M. B. Chadwick, P. Obložinský, M. Herman, N. M. Greene, R. D. McKnight, D. L. Smith *et al.*, Nucl. Data Sheets **107**, 2931 (2006).

[23] L. McFadden and G. R. Satchler, Nucl. Phys. **A84**, 177 (1966).

[24] M. Blann and H. K. Vonach, Phys. Rev. C **28**, 1475 (1983).

[25] H. Vonach, M. Uhl, B. Strohmaier, B. W. Smith, E. G. Bilpuch, and G. E. Mitchell, Phys. Rev. C **38**, 2541 (1988).

[26] V. Avrigeanu, T. Glodariu, A. J. M. Plompen, and H. Weigmann, J. Nucl. Sci. Technol. Suppl. **2**, 746 (2002); http://tandem.nipne.ro/ vavrig/Publications/2002/Tables/.

[27] Evaluated Nuclear Structure Data File (ENSDF), http://www.nndc.bnl.gov/ensdf/index.jsp.

[28] IAEA-CRP Reference Input Parameter Library (RIPL-2), http://www-nds.iaea.or.at.

[29] A. V. Ignatyuk, G. N. Smirenkin, and A. S. Tishin, Yad. Fiz. **21**, 485 (1975); Sov. J. Nucl. Phys. **21**, 255 (1976).

[30] A. R. Junghans, M. de Jong, H.-G. Clerc, A. V. Ignatyuk, G. A. Kudyaev, and K.-H. Schmidt, Nucl. Phys. **A629**, 635 (1998).

[31] A. J. Koning and M. B. Chadwick, Phys. Rev. C **56**, 970 (1997).

[32] M. Avrigeanu and V. Avrigeanu, Comput. Phys. Commun. **112**, 191 (1998); A. Harangozo, I. Stetcu, M. Avrigeanu, and V. Avrigeanu, Phys. Rev. C **58**, 295 (1998).

[33] E. Gadioli and E. Gadioli-Erba, Z. Phys. A **299**, 1 (1981).
[34] J. Pampus, J. Bisplinghoff, J. Ernst, T. Mayer-Kuckuk, J. Rama Rao, G. Baur, F. Rosel, and D. Trautmann, Nucl. Phys. **A311**, 141 (1978).
[35] H. I. West, Jr., R. G. Lanier, and M. G. Mustafa, Phys. Rev. C **35**, 2067 (1987).
[36] N. Yamano, Table of Isotope Production Cross Sections (ACSSELAM Library), http://wwwndc.jaea.go.jp/ftpnd/sae/acl.html.
[37] G. B. Liu and H. T. Fortune, Nucl. Phys. **A496**, 1 (1989); EXFOR T0064 data file entry; T. Yanabu, S. Yamashita, T. Nakamura, K. Takamatsu, A. Masaike, S. Kakigi, D. C. Nguyen, and K. Takimoto, J. Phys. Soc. Jpn. **17**, 914 (1962); EXFOR E1873 data file entry.